ACCOUNTS
of chemical research

Supracrystals of Inorganic Nanocrystals: An Open Challenge for New Physical Properties

M. P. PILENI

Laboratoire LM2N, Université P. et M. Curie (Paris VI), BP 52, 4 Place Jussieu, F-75231 Paris Cedex 05, France

RECEIVED ON MARCH 10, 2008

CONSPECTUS

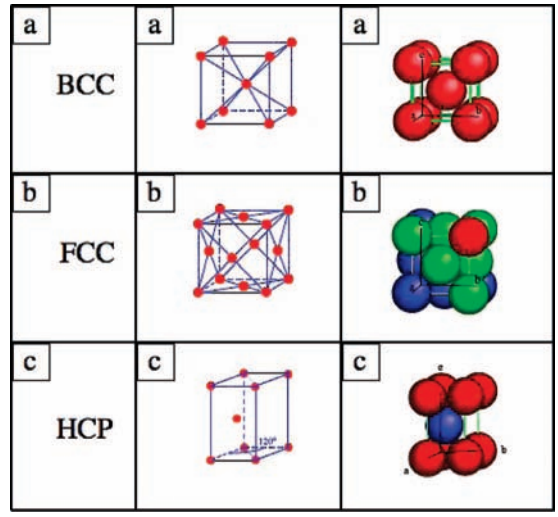

When naturally occurring spherical objects self-organize, the physical properties of the material change. For example, a colorless opal is the result of a disordered aggregate of silica particles. When the silica particles are ordered, however, the opal takes on color, which is determined by the size of the self-assembled particles.

In this Account, we describe how these 3D arrangements of nanomaterials can self-organize in 3D arrays called supracrystals; the 3D arrays can fall into the familiar categories of face-centered cubic (fcc), hexagonal compact packing (hcp) crystals, and body-centered (bcc) crystals. The collective properties of these 2D and 3D arrangements are different from the properties of individual nanoparticles and from particles in bulk.

Comparison between the approach to saturation of the magnetic curve for supracrystals and disordered aggregates produced from the same batch of nanocrystals is similar to that observed with films or nanoparticles, either highly crystallized or amorphous. We also demonstrate by two various processes and with two types of nanocrystals (silver and cobalt) that when nanocrystals are self-ordered in 3D superlattices, they exhibit a coherent breathing mode vibration of the supracrystal, analogous to a breathing mode vibration of atoms in a nanocrystal.

Furthermore, we used 10 nm γ-Fe_2O_3 nanocrystals to gain new insight into the scaling law of crack patterns. We found that isotropic and directional crack patterns follow the same universal scaling law over a film height varying by 3 orders of magnitude.

These data have led us to propose general analogies between supracrystals of nanocrystals, individual nanocrystals, and the molecules in the bulk phase for certain physical properties based on the ordering of the material. As we continue to study the physical properties of the ordered and disordered arrangements of nanomaterials, we will be able to go further in these analogies. And this exploration leads to new questions: first and foremost, is this behavior general?

Introduction

Nanoscience is old as the world. In fact, nanomaterials are synthetized in a rather large number of animals and bacteria,[1] and they have been used for more than 2000 years as dyes in painting because their colors differ with their sizes and shapes.[2]

Spherical objects like balls or nanomaterials having a uniform diameter self-organize in com-

Published on the Web 11/13/2008 www.pubs.acs.org/acr
10.1021/ar800082q CCC: $40.75

pact hexagonal networks (2D). The stacking of these layers (3D) makes possible formation of face-centered cubic (fcc) and hexagonal compact packing (hcp) crystals.[3−5] In these, as well as body-centered cubic (bcc) crystals, the atoms are regularly arranged; disordered atoms make up solids called "amorphous". In many crystalline phase diagrams of bulk metals, depending on the temperature and pressure, two phases are obtained.[6,7] The nanocrystal crystalline structures can be tuned either with their sizes[8,9] or the pressure.[10] Even if the forces involved are not the same, an analogy of balls, nanomaterials, and atoms can be made with formation of similar structures. In the following, supracrystal is the name for nanomaterials that have a low size distribution (rather uniform) and are self-ordered in various structures (fcc, hcp, bcc).

Silica particles (micrometer sizes) forming either disordered or ordered aggregates show marked changes in their optical properties. For example, a colorless opal is an opal made of disordered particles, whereas when the particles are ordered, specific reflectivity related to the size of the self-assembled particles is observed.[11] The change in the opal color is due to size segregation of the self-ordered silica particles. From this change in the optical properties with the ordering of large particles, it can be assumed that intrinsic properties can be expected when nanocrystals are ordered or not in a supracrystal.

To demonstrate these intrinsic behaviors, we need to produce, from the same batch of nanomaterials, either disordered aggregates or supracrystals. Several intrinsic properties have been observed in the past few years.[12] For example, well-defined columns of nanocrystals self-ordered in fcc supracrystals are produced when a magnetic field is applied perpendicular to the substrate during the evaporation whereas labyrinths are formed with polydispersed nanocrystals. Similarly, a change in the distribution of the dipolar interaction energies is observed when cobalt nanocrystals are ordered in fcc supracrystals. Due to the nanocrystal ordering, there is a new crystalline growth mechanism with formation of well-crystallized triangular single silver crystals with a size controlled by that of the initial nanocrystal ordering range.

Collective optical and magnetic properties due to dipolar interactions are observed when the nanocrystals are organized in 2D superlattices.[13] The optical properties of 5 nm silver nanocrystals organized in hexagonal networks give rise to several plasmon resonance modes, which are attributed to the film anisotropy. In the magnetic properties, the hysteresis loop of nanocrystals is squarer when they are deposited in compact hexagonal networks than that seen with isolated nanocrystals. Also the calculated and experimental hysteresis loops

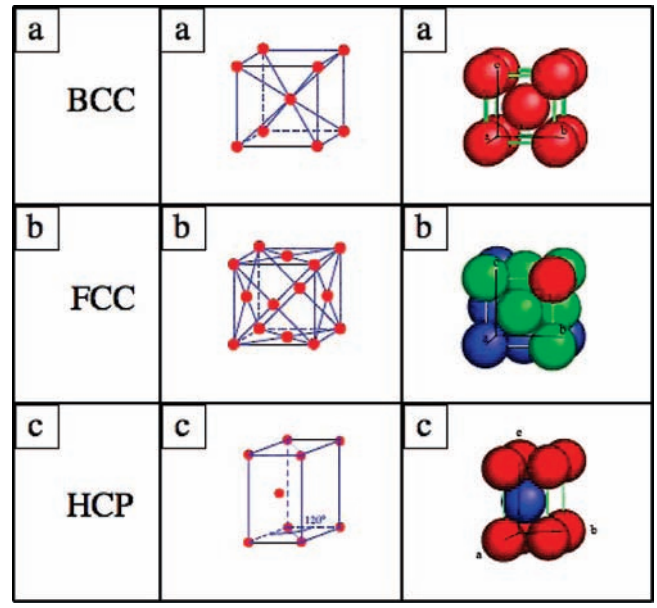

FIGURE 1. Sketch of atom-ordering in bcc (a), fcc (b), and hcp (c) structures.

for a chain-like structure are squarer than that of a well-ordered array of nanocrystals. The linear chains of nanocrystals behave as homogeneous nanowires as in the magnetostatic bacteria.[1]

Here we describe new intrinsic properties obtained with silver and cobalt nanocrystals with average sizes of 5 and 6.5 nm and 12% average size distribution. Silver nanocrystals are able to self-assemble into supracrystals in two structures, such as fcc and hcp or hcp and bcc supracrystals, at a fixed pressure and various temperatures. Comparison of the hysteresis loops of supracrystals and disordered aggregates of cobalt nanocrystals shows that they are similar to those observed with highly crystallized and amorphous films and also amorphous and crystalline nanoparticles. The coherence breathing between nanocrystals produced with either silver or cobalt nanocrystals in a supracrystal is a general behavior. We demonstrate also that the use of 10 nm γ-Fe_2O_3 nanocrystals enables new insights for the scaling law of crack patterns. Isotropic and directional crack patterns made of nanocrystals follow the same universal scaling law with the film height varying by 3 orders of magnitude.

Tune the Various Packing Structures in 3D Superlattices of Silver Nanocrystals

We know that atoms in bulk phase metals and in nanocrystals are either ordered in various crystalline structures such as bcc (Figure 1a), fcc (Figure 1b), or hcp (Figure 1c) or disordered with the formation of so-called amorphous material. The phase diagrams, depending on temperature and pressure,

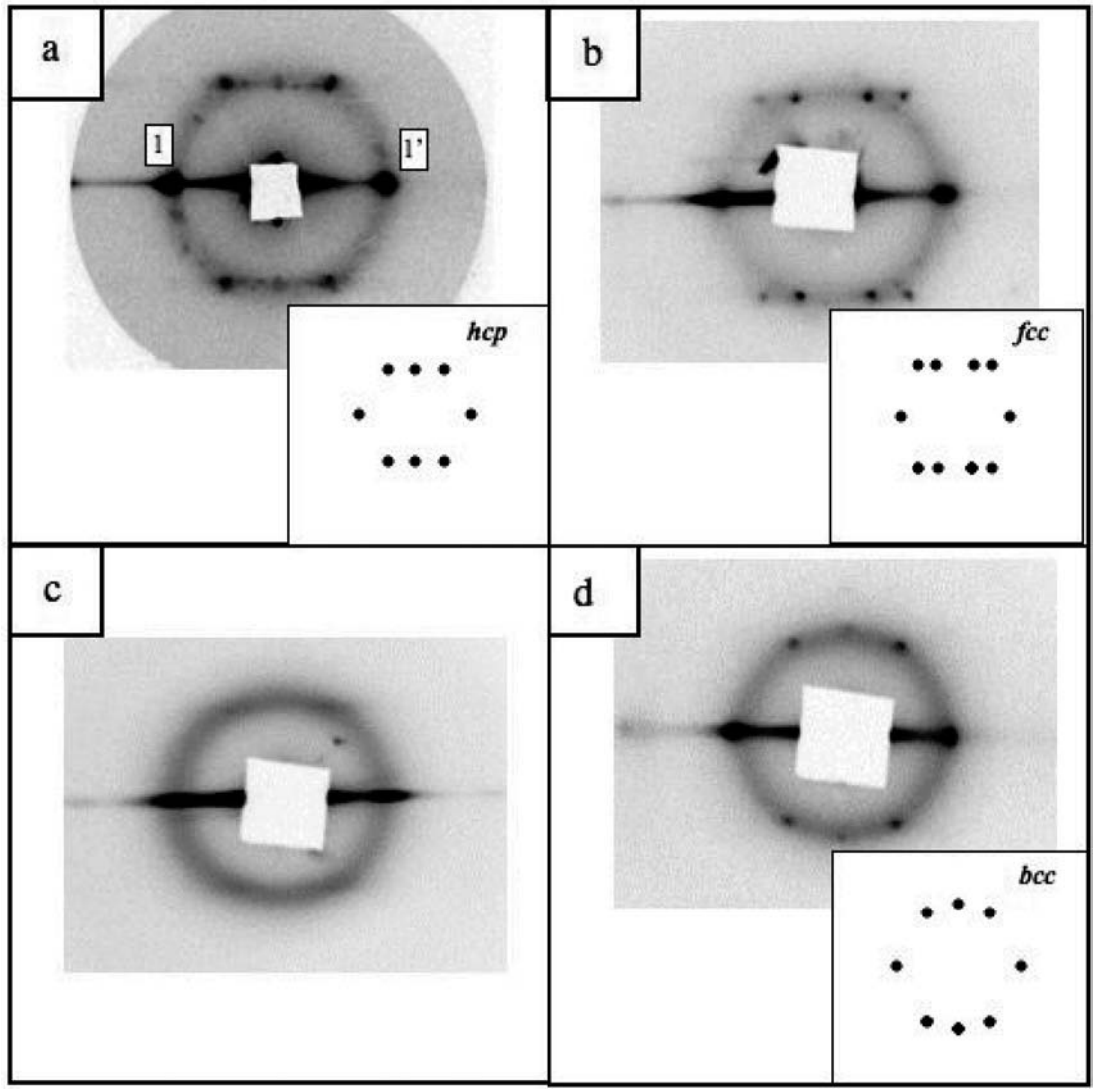

FIGURE 2. Small-angle X-ray diffraction patterns corresponding to Ag−C_{10} nanocrystals initially dispersed in decane, evaporated at 15 (a) and 50 °C (b) and to Ag−C_{12} nanocrystals initially dispersed in decane evaporated at 15 (c) and 50 °C (d). The insets are the corresponding simulated diffraction patterns.

show mainly two of these three crystalline structures.[5] In the following, we report that similar behavior is observed in a supracrystal of nanocrystals. In the past few years, we demonstrated that it is possible to produce with the same batch of nanocrystals coated with dodecanethiol ligands and dispersed in hexane either disordered aggregates or fcc supracrystals[12] several micrometers thick. Silver nanocrystals having the same average diameter (5 nm) and size distribution (12%) coated by either decanethiol or dodecanethiol [called Ag(C_{10}) and Ag(C_{12})] and dispersed in decane are kept in a beaker with a substrate at its bottom. By solvent evaporation (8 days), the nanocrystals are deposited on the temperature-controlled substrate with no control of the solvent temperature. The small-angle X-ray diffraction (SAXRD) pattern (Figure 2a) of Ag(C_{10}) nanocrystals deposited on the 15 °C substrate shows two strong reflections (numbered 1 and 1′ in Figure 2a) normal to the substrate. The width of the first-order Bragg reflection is nearly resolution-limited indicating long-range ordering of the nanocrystals perpendicular to the surface. Other less intense spots are also observed in this pattern revealing a three-dimensional long-range ordering within supracrystalline domains. The corresponding simulated diffraction pattern shown in the Figure 2a inset gives unambiguous evidence for hcp packing. The experimental and calculated diffraction spot coordinates fit very well and enable indexing of the diffraction pattern.[14] On increasing the substrate temperature to 25 °C, the diffraction pattern is typical of silver nanocrystal fcc packing with the (111) plane lying parallel to the substrate. A further increase in the substrate temperature to 50 °C improves the crystallinity of supracrystals with a marked

decrease in the defects (Figure 2b). These structures are attributed to equilibrium states because they do not depend on the solvent evaporation rate.[15] Our results show that an increase in the substrate temperature from 15 to 25 °C is enough to induce the hcp-to-fcc transition. The temperature increase modifies the steric repulsions between the alkyl chains as it modifies their mobility. This probably changes the free energy of the system and thus induces the hcp−fcc phase transition. Hence, with the same nanocrystals dispersed in a given solvent, the two structures, as in the bulk metallic phase and with a very small difference in the free energy, can be produced. The transitions from hcp to fcc supracrystals are produced by changing the substrate temperature as in the various bulk phase diagrams.

When Ag(C_{10}) is replaced by Ag(C_{12}) keeping the same experimental conditions, the crystallinities of the supracrystals markedly differ: The diffraction pattern observed when the substrate temperature is 15 °C during the evaporation process, Figure 2c, shows a halo larger than the experimental resolution indicating that disordered aggregates are produced. On increasing the substrate temperature to 25 and 35 °C, the diffraction patterns display several diffraction spots typical of a compact structure corresponding to hcp with more or fewer defects. On further increasing the substrate temperature to 50 °C, the diffraction pattern markedly changes and displays diffraction spots typical of a bcc arrangement (Figure 2d).[15] This is confirmed by the corresponding simulated diffraction pattern in the Figure 2d inset. In this case, it is possible to obtain different crystalline structures such as hcp containing more or fewer defects and bcc and also amorphous materials. Note that bcc is in thermodynamic equilibrium and is obtained by using, as coating agent, an alkyl chain that is longer by two carbon atoms. The solid phase diagram of Ag−C_{12} is clearly different from that of Ag−C_{10} and includes hcp, compact structure, and bcc lattices. The stability of the coated silver nanocrystals does not depend only on the hard-core repulsion between the cores but also on the interaction between the thiol coronas. The soft corona is known to favor structures that minimize the interfacial energy favoring the loose structure (bcc), and the hard cores are known to favor lattices with high packing fractions. The true ground-state is determined by balancing these two competing tendencies. The presence of hydrocarbon chains between the particles clearly modifies the delicate balance between these interactions. Indeed, the interdigitation between the alkyl chains reduces their orientational entropy within the corona, which gives rise to a short-range repulsive interaction. Nanocrystal assembly is controlled primarily by hard-core repulsion. In this case, to a first approximation, dense lattices such as fcc or hcp are favored. When the interparticle distances D increase, the repulsive interactions, which are at short-range, vanish. Then, the assembly becomes controlled by the soft coronas, and loose and more open lattices such as the bcc are favored. This suggests that Ag nanocrystals form dense superlattices by virtue of the interdigitation of the neighboring alkyl chains. The dynamics of the C_{12} chains rises abruptly at the melting temperature (52 °C). At this temperature, 70% of the chains are found to be dynamic. Thus they cannot take part in the interdigitation and induce the formation of loose Ag−C_{12} superlattices. The dynamics of shorter chains evolves progressively with the temperature. When the temperature increases, the proportion of alkyl chains participating in the dynamics increases, and at 127 °C, all the chains participate (in the dynamics). This agrees with dense superlattices (hcp, fcc) up to 50 °C for AgC_{10} and up to 35 °C for Ag−C_{12}. Above 35 °C, more open Ag−C_{12} superlattices like the bcc are observed. Thus, silver nanocrystals, characterized with a given coating agent and dispersed in decane, grow into supracrystals having various structures. The change in the structure is tuned by changing either the coating agent, by only two carbon atoms, or the temperature. Similarly, disordered aggregates of nanocrystals are produced as when the atoms are disordered in bulk or nanoparticle phases (amorphous materials). From this, an analogy with atoms in a bulk phase or in nanocrystals can be made with the appearance of two crystalline structures of the supracrystals by changing the temperature during the deposition process.

Magnetic Properties: Nanocrystals Ordered or Not in a Supracrystal Behave as Atoms and Nanocrystals in the Bulk Phase

Here we compare the magnetic response of disordered aggregates (Figure 3a) with that of fcc supracrystals (Figure 3b) produced from the same batch of nanocrystals. Figure 3c shows the magnetization versus field curves for the ordered and disordered 3D cobalt nanocrystal assemblies. We observe that for the supracrystals the approach to saturation is more gradual than for the disordered aggregates. This difference is explained by considering the model of amorphous ferromagnets proposed by Chudnovsky et al.[16,17] In this model, there is only short-range structural order that leads to a local random anisotropy with a short-range correlation length. The randomness of this local anisotropy leads to a very small uniform anisotropy in the sample, referred to as coherent anisotropy. The model predicts an approach to saturation in these materials given by $DM \cong 1/H^{1/2}$, which has been confirmed experimentally.[18]

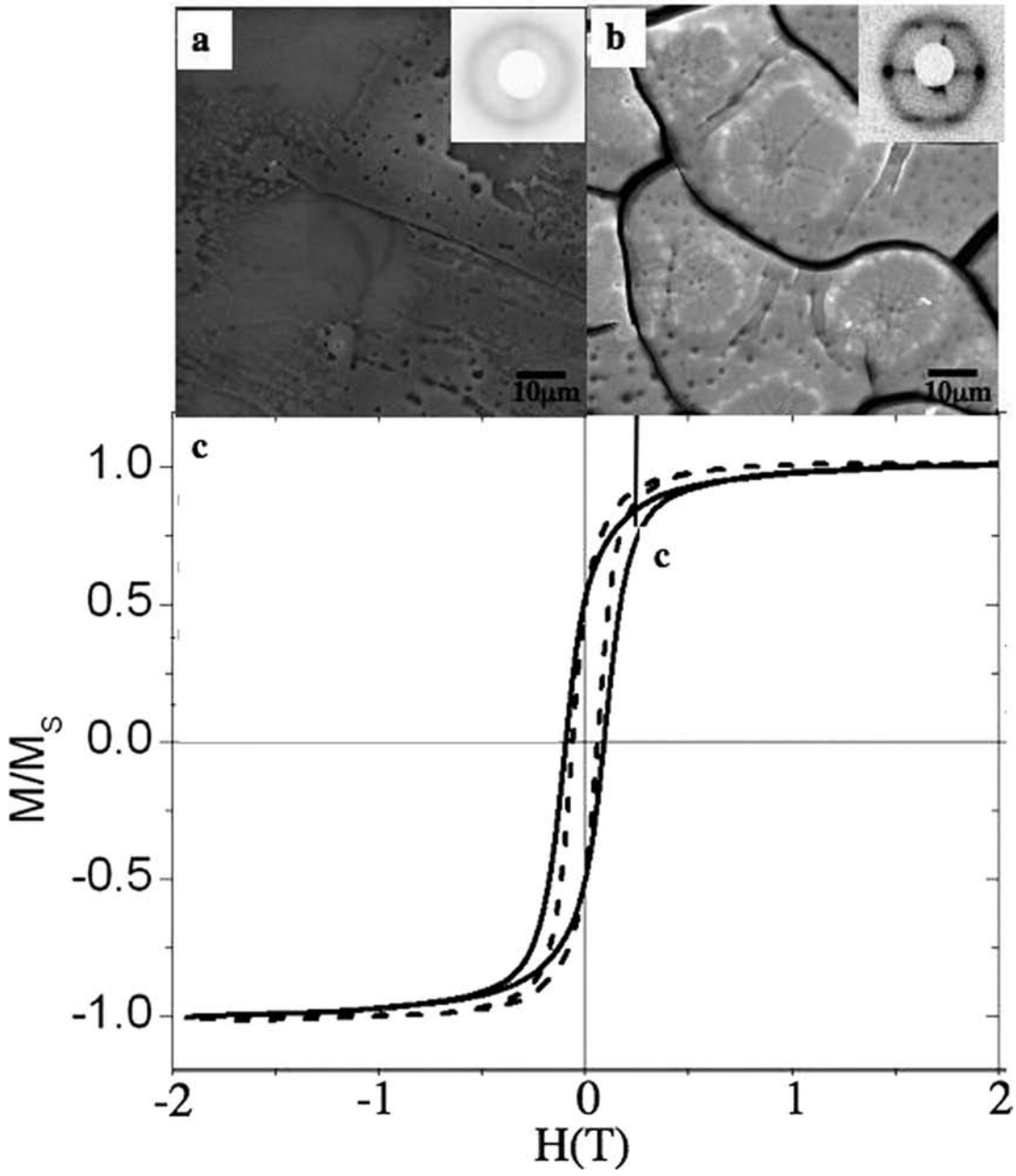

FIGURE 3. SEM image of fcc supracrystals (a) and amorphous aggregates (b) of 7 nm cobaltnanocrystals and (c) M/M_s versus H curves of disordered (dashed line) and ordered (solid line) 3D assemblies.

This was extended to disordered nanocrystallized films,[19] where a $1/H^{1/2}$ approach to saturation is also observed. In addition, the authors show that increasing the anisotropy in these films leads to a deviation from $1/H^{1/2}$ to $1/H^2$ on approaching saturation, which would apply in the case of a perfect, uniaxial system. By analogy to what is observed in Figure 3c, it is concluded that in the disordered aggregates, the direction of anisotropy randomly fluctuates from one magnetic nanocrystal to another and leads to an extremely small uniform local anisotropy with a square root magnetization law on approaching saturation. For supracrystals, due to long-range mesoscopic order, the total anisotropy is rather large with internanocrystal coupling energies leading to a smoother magnetization curve on approaching saturation. This clearly shows that the magnetic properties of ordered and disordered aggregates of nanocrystals[20] behave similarly to those of highly crystallized and amorphous materials. Similarly, as predicted, the coercive field increases for supracrystals (900 Oe) compared with disordered aggregates (600 Oe). Again, as above, this agrees

with a change in the local anisotropy with the nanocrystal ordering.[18] From this comparison between the approach to saturation magnetization and the hysteresis loop of either amorphous material or highly crystallized supracrystals, it is reasonable to conclude that there is a similarity in the magnetic behavior between disordered aggregates and highly ordered supracrystals as in amorphous and highly crystalline materials of atoms. To go further, to a first approximation, we could assume that the magnetic behavior of atoms and nanocrystals is similar in a given order.

Coherent Vibrations of Nanocrystals Self-Ordered in Supracrystals as Atoms in a Nanocrystal

The low-frequency Raman spectra of silver nanocrystals show a very intense peak attributed to the excitation of the quadrupolar vibrational mode of the nanocrystals via the plasmon−phonon interaction. For spherical nanocrystals with sizes larger than ~1 nm, the frequencies are given by the following equation:[21]

$$\nu = \frac{S_{\ln}\nu_t}{D} \quad (1)$$

where $S_{\ln}$ depends on the ratio ν_l/ν_t. The line shape agrees with the inverse size histogram because the intensity of Raman scattering frequency is inversely proportional to the nanocrystal diameter. This is observed with disordered silver nanocrystal aggregates, [22] as with nanocrystals dispersed in a matrix.[23] This indicates intrananoparticle coherence; that is, the atoms in the nanocrystals coherently vibrate.

When fcc supracrystals are small enough (size < λ/10, where λ is the laser excitation wavelength) and characterized by a rather large number of defects with slightly diffuse spots in the small-angle X-ray diffraction pattern (Figure 4a), the light is scattered by stationary modes, which are the supracrystal vibration eigenmodes, as by the vibration modes of a molecule. The active vibration modes are regarded as localized, and they are determined only by their symmetry. In consequence, the selection rule for the phonon momentum vector does not limit the Raman active vibration mode number, so the intensity of Raman scattering from a supracrystal, $I_{sc}(\nu)$, is

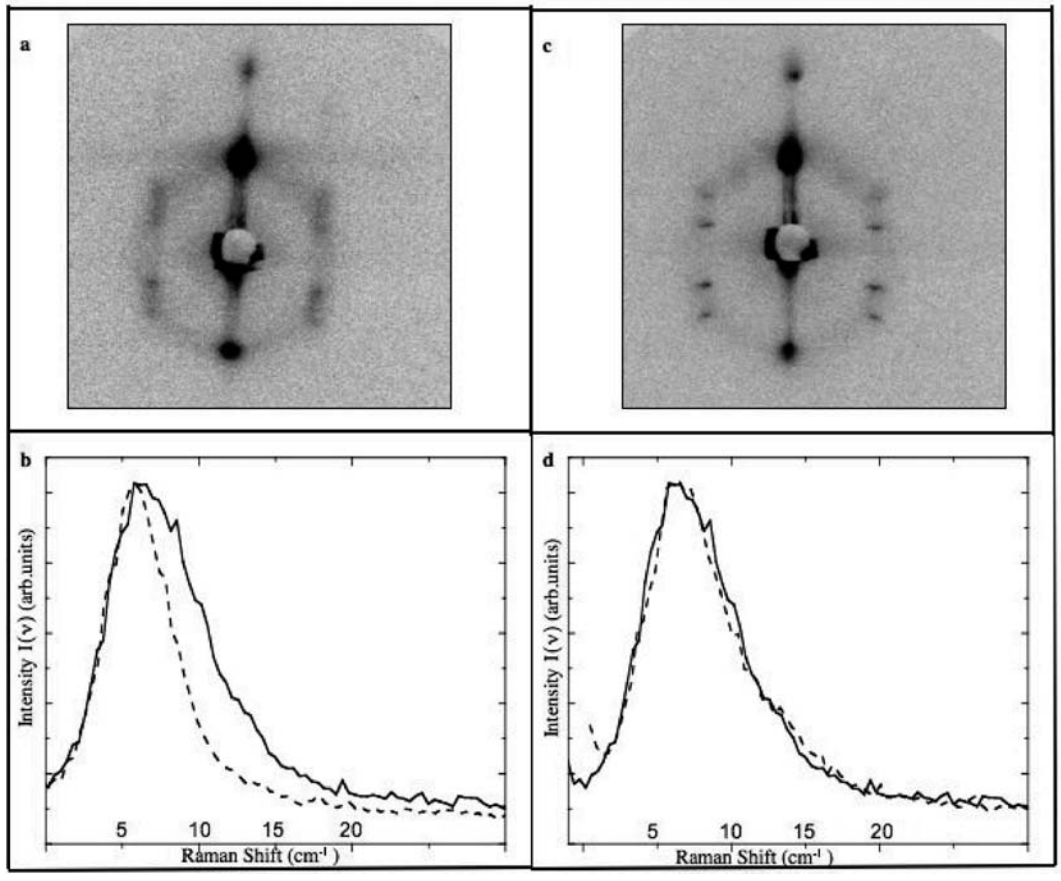

FIGURE 4. (a) SAXRD pattern of small supracrystals, (b) low-frequency Raman spectra from disordered assemblies (solid line) and small supracrystals (dashed line) of silver nanocrystals, (c) XRD pattern of large supracrystals, and (d) the corresponding low-frequency Raman spectra from disordered assemblies (solid line) and small supracrystals (dashed line) of silver nanocrystals

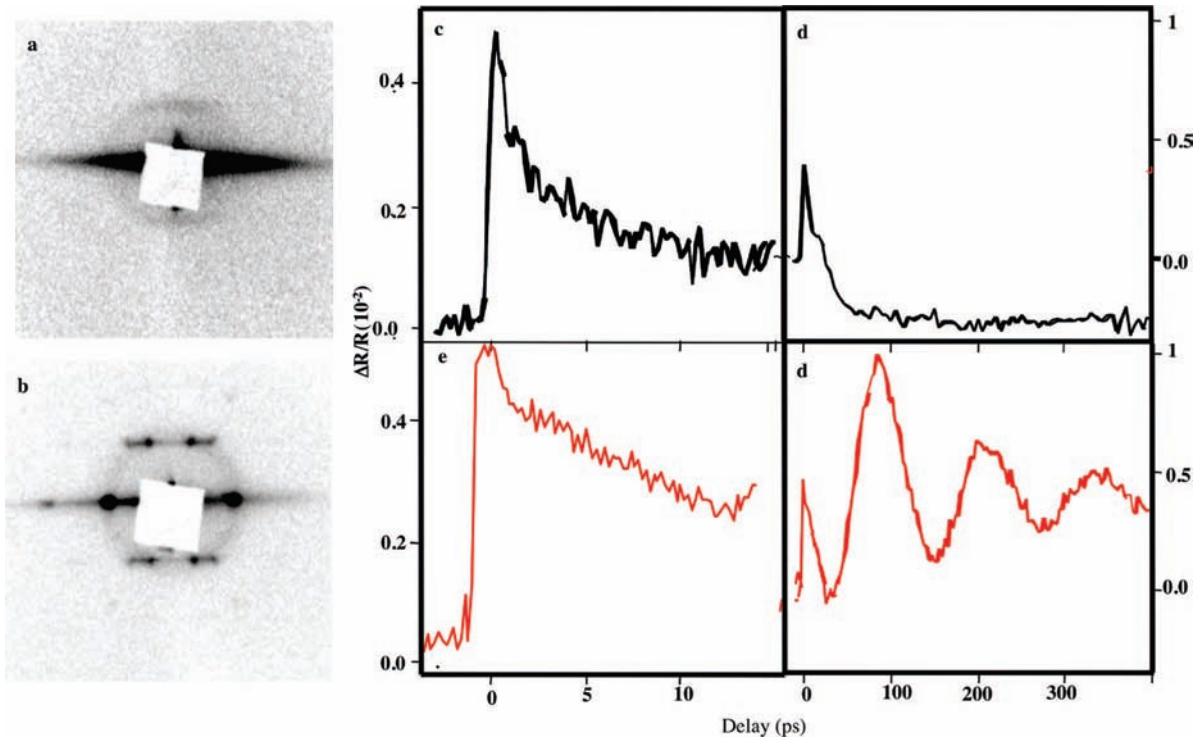

FIGURE 5. Differential reflectivity dynamics of assemblies of 6.3 nm cobalt nanocrystals: (a) GISAXS pattern of disordered aggregates of 6.3 nm cobalt nanocrystals, (b) GISAXS pattern of supracrystals of 6.3 nm cobalt nanocrystals, (c) short time range corresponding to disordered aggregate, (d) short time range corresponding to fcc supracrystals, (e) long time range corresponding to disordered aggregate, (f) long time range corresponding to fcc supracrystals.

proportional to the square of that of nanocrystal amorphous aggregates, $I(\nu)$ as in[24]

$$I_{sc}(\nu) \propto L^2(\nu)F^2(\nu) \propto L^2(\nu)I^2(\nu) \quad (2)$$

As expected, the Raman peak bandwidth is narrower for small supracrystals than for disordered aggregates (Figure 4b). And, as expected from eq 2, the experimental peak of the supracrystals has the same profile as the square of the disordered aggregates[22] indicating internanocrystal coherence inside fcc supracrystals.

For large fcc supracrystals (size > $\lambda/10$) characterized by a well-defined diffraction pattern (Figure 4c), the Raman intensity $I_{sc}(\nu)$ due to vibrations in large supracrystals is proportional to the Raman intensity of amorphous aggregates:[24]

$$I_{sc}(\nu) \propto L^2(\nu)I(\nu) \quad (3)$$

Hence, the Raman peak shape, in the case of large supracrystals, is like that observed for disordered nanocrystal assemblies. As expected from the model,[24] the bandwidth of the Raman peak is similar to that obtained with amorphous aggregates of nanocrystals (Figure 4d). This does not prove that there is vibrational coherence in large supracrystals. However, the fact that there is no change in the Raman peak between large supracrystals and disordered aggregates means that vibrational coherence of nanocrystals in supracrystals cannot be observed. But, as mentioned above, this is possible with small supracrystals. From these data, it is concluded, because the model predicts such behavior and the experiments agree, that for any supracrystal size, there is vibrational coherence between nanocrystals in a supracrystal. This coherence breathing is because the van der Waals bonding between thiol chains is sufficient to establish a correlation between the vibrating nanocrystals, so that they vibrate coherently in a supracrystal.

To give a direct proof of this breathing property of nanocrystals in a supracrystal and to demonstrate that this is a general behavior, we use cobalt instead of silver nanocrystals and femtosecond laser pulse pump−probe spectroscopy.[25] As described above, the same procedure is followed to produce, from the same batch of cobalt nanomaterials, either disordered aggregates (Figure 5a) or supracrystals (Figure 5b) After the pump pulse excitation, the femtosecond electron dynamics[26] are described by an initial athermal distribution, which thermalizes within a few hundreds of femtoseconds into a hot electron distribution via electron−electron scattering. The electrons then relax to the lattice via the electron−phonon interaction with a characteristic time τ_{e-p}. This relaxation time is 3 ps (Figure 5c) and

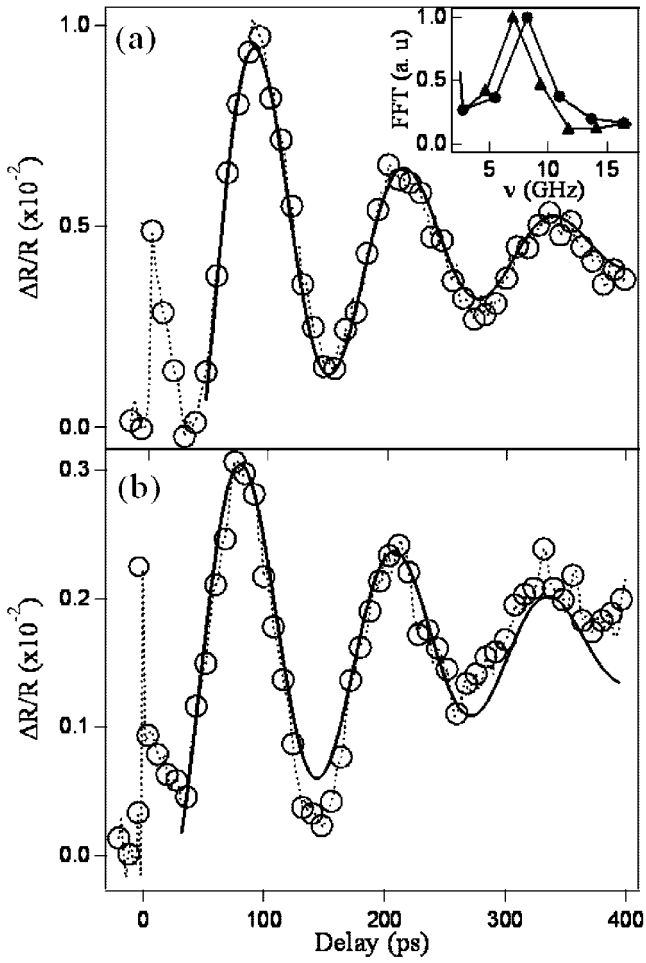

FIGURE 6. Long-range differential reflectivity dynamics of 6.3 nm (a) and 7.3 nm (b) cobalt nanocrystals self-assembled in supracrystals (solid line is the fit from the model). Inset contains Fourier transforms of the oscillation frequency.

7 ps (Figure 5d) for disordered and fcc ordered aggregates, respectively. This is consistent with the time scale of the electron−lattice relaxation in polydispersed cobalt nanoparticles implanted in a dielectric matrix.[27] On a picosecond to nanosecond time scale, the energy deposited by a pump pulse dissipates into the environment of the nanocrystals. This can be described by a thermal diffusion mechanism. The reflectivity dynamics for the disordered aggregates on the bare substrate do not show any modulation (Figure 5c) whereas large oscillations with a characteristic period $\tau_{osc} = 125$ ps corresponding to a low frequency mode of 1.7 cm^{-1} are observed with fcc cobalt supracrystals (Figure 5d).[25] The van-der-Waals interactions between nanocrystals are strong enough to allow the energy to dissipate via the interdigitated aliphatic chains. It is therefore a coherent motion of the entire supracrystal of cobalt nanocrystals linked by the chains. Probably due to structural defects in the supracrystals, the oscillations damp faster than the heat diffusion time. A simple description model consists of spheres (cobalt nanocrystals) characterized with a mass m, interconnected by springs (aliphatic chains) with a rigidity constant k. A similar model is often used for describing the vibrations of an atomic crystal.[28] The frequency of this harmonic oscillator is $\omega_{osc} = 2(k/m)^{1/2}$. Figure 6a,b represent the oscillations of the supracrystal for the 6.3 nm and 7.3 nm diameter nanocrystals, respectively. The inset in Figure 6a displays their Fourier transforms showing a slight change in the oscillation frequency $f_{osc(d=6.3nm)} = 8.2$ GHz and $f_{osc(d=7.3nm)} = 7.1$ GHz. Figure 6 also shows the best fit obtained assuming a damped oscillator model:

$$\Delta R(t)/R = A\, e^{-t/\tau} \cos[\omega_{osc}(t - t_0)]$$

For the 6.3 nm nanocrystals ($m = 2.28 \times 10^{-21}$ kg), the rigidity constant k is deduced from ω_{osc} and is 1.4 N/m. This is the rigidity of the bundles of interdigitated dodecanoic acid chains linking two nanocrystals. This value can be compared with that estimated from the compressibility modulus of such a chain, $K_m = 10^8$ N/m^2. The number of dodecanoic chains per nanocrystal is estimated to be 190 molecules, contributing to 12 connections with neighboring nanocrystals in the fcc supracrystals. This is deduced from the surface area per polar headgroup of the coating agent (0.5 nm^2) and the coverage ratio for a 6.3 nm cobalt nanocrystal (75%). Hence there are 16 chains per connection corresponding to an area $A = 8$ nm^2. The strength of the connection is therefore $K_m A = 8 \times 10^{-10}$ N, which leads to a compressibility of 0.9 N/m for the connections if we consider that the spring is only the interdigitation zone of ~0.9 nm. It is 0.27 N/m if we consider that all the chains between the two nanocrystals act as a spring: 3 nm. These rigidity values are in good agreement with that deduced from our experimental results (1.4 N/m). For the 7.3 nm diameter nanocrystals supracrystal, similar modulation of $\Delta R(t)/R$ is observed with a characteristic period $\tau_{osc} = 131 \pm 5$ ps. This allows checking the validity of our model: the period depends both on k (1.8 N/m deduced from ω_{osc}) and m ($\tau_{osc} \propto (m/k)^{1/2}$). A variation of the diameter induces a variation of m, which varies with the volume $\sim d^3$, whereas k depends on the surface $\sim d^2$ (number of chains in the connection). Therefore, $\Delta\tau_{osc}/\tau_{osc} = {}^1/_2(\Delta d/d)$. A variation of 1 nm in the diameter d corresponds to a change of 7% in the oscillation period τ_{osc}, which is in very good agreement with the experimental values (133 ps vs 131 ps).

The similarity between what was observed with atoms and nanocrystals in their crystalline form allows us to claim that nanocrystals when they are ordered in a supracrystal breathe

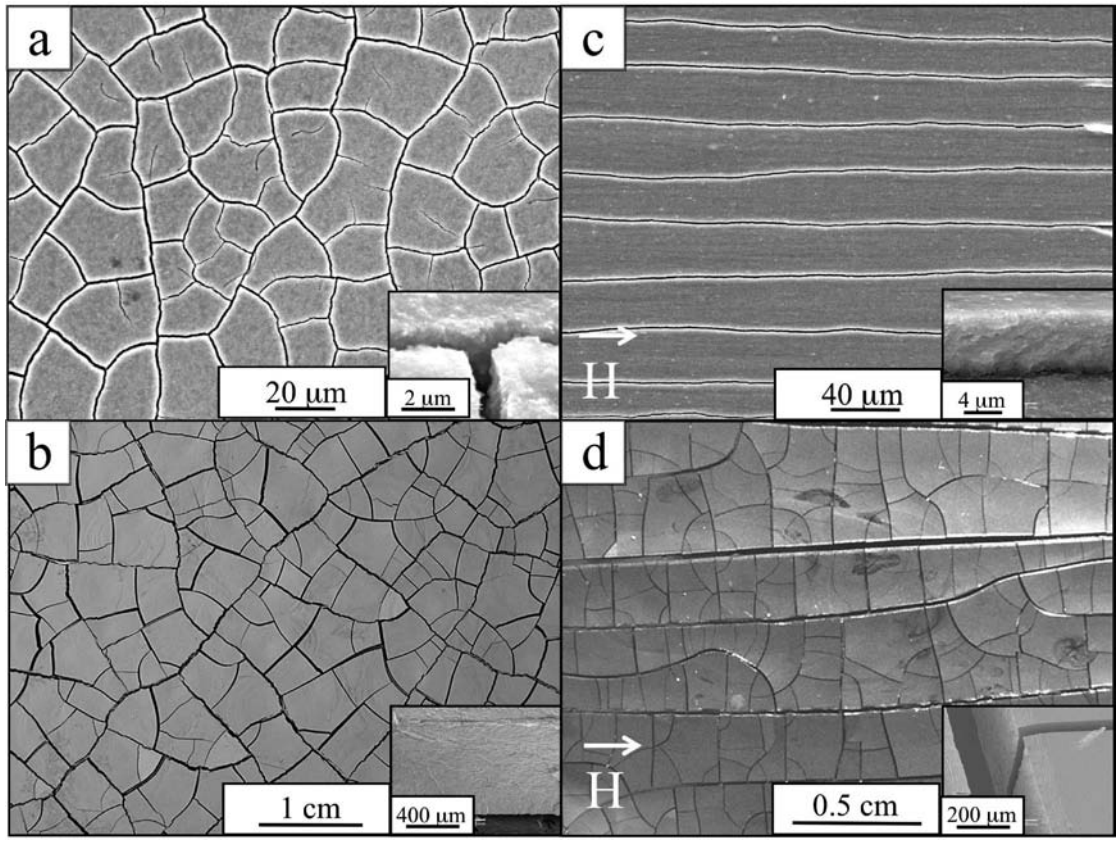

FIGURE 7. SEM (a, c) and photographic (b, d) images of isotropic (2D) and directional (1D) crack patterns (made) of 10 nm γ-Fe_2O_3 nanocrystals. Insets show SEM images at 45° tilt. (a, c) Micrometric-size 2D and 1D crack patterns; (b, d) centimeter-size 2D and 1D crack patterns.

coherently as atoms in nanocrystals. From the fact that this property has been oberved by two different techniques (Raman scattering and time-resolved spectroscopy) and with two different types of nanomaterials (silver and cobalt nanocrystals), we claim that collective vibrations of nanocrystals in supracrystals exist and that these behave as atoms in a nanocrystal.

Cracks in Nanocrystal Films Could Follow a Universal Behavior?

At the mesoscopic range, the film made of supracrystals has cracks. We ask how cracks could be avoided. In fact, cracks due to a shrinking film restricted by adhesion to a surface have been studied over several decades.[29] They are observed in nature at various length scales ranging from tiny crack segments in nanocrystal films to enormous domains observed in the earth's crust.

In the following, we describe crack patterns obtained by injecting 10 nm γ-Fe_2O_3 nanocrystals dispersed either in water or in chloroform above a silicon wafer placed at the bottom of a glass beaker. During the solvent evaporation at room temperature, the solution is subjected or not to an applied magnetic field (0.2 T) parallel to the substrate. Crack patterns appear after drying. Their sizes (from micrometers to centimeters) are controlled by the nanocrystal concentrations.[30]

In absence of an applied magnetic field, at low nanocrystal concentrations, isotropic 2D cracks are produced at the micrometer scale (Figure 7a), whereas crack patterns at the centimeter scale are obtained at high concentrations (Figure 7b). Very surprisingly below a film thickness of 2 μm, no individual fragments bounded by cracks are produced. On increasing the volume and nanocrystal concentrations, the heights of the cracks increase from $H = 2.8$ μm (Figure 7a) to $H = 1$ mm (Figure 7b). As already observed,[29] the distribution of crack junction angles is peaked at 90° for any film thickness, and the crack domains are mainly four-sided with six neighbors. A linear variation, on a logarithmic scale, of the average square root area of crack domains ($A^{1/2}$), ignoring secondary cracks as explained in ref 30, with the layer height is observed (filled circles in Figure 8). The linear fit gives a slope of 0.99 in good agreement with a universal scaling law, $A = (KH)^2$, with the dimensionless ratio $K = A^{1/2}/H$ equal to 5.42. The scaling law is shown over 3 orders of magnitude.

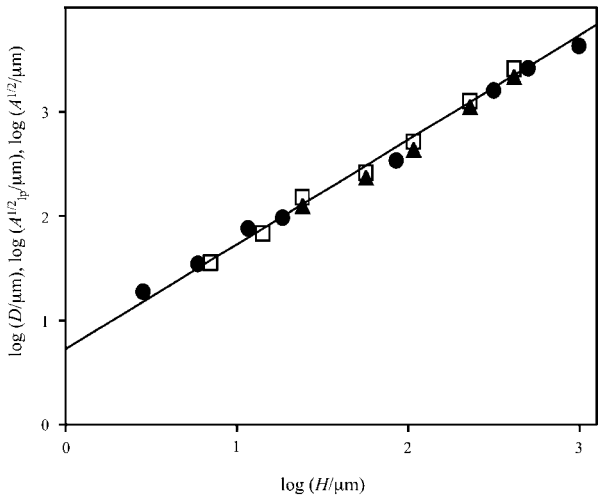

FIGURE 8. Dependence of the average crack distance (D) and the average square root areas of isotropic and directional 2D cracks ($A^{1/2}$, $A_{lp}{}^{1/2}$) on the layer height.

By application of a magnetic field during the drying process, linear cracks spanning the whole substrate are observed. As above, the size of the crack patterns depends on the initial concentration of nanocrystals deposited with formation of directional cracks at the micrometer (Figure 7c) and centimeter scale (Figure 7d). When the nanocrystal volume and concentration are increased before drying, the average distance between regular linear cracks, D, varies from 35 to 2590 μm with the film height ($H = 7$ μm (Figure 7c) to 415 μm (Figure 7d)) The straight cracks parallel to the direction of the applied field correspond to the first generation of cracks and are called primary 1D cracks. The fragments bounded by these primary 1D cracks and the perpendicular ones (second generation of cracks) are called primary 2D cracks. A linear variation, on the logarithmic scale, of the average crack distance (D) between primary cracks and the corresponding height (H) is observed (squares in Figure 8). The linear fit gives a slope of 1.00. This leads to the scaling law, $D = KH$ with the dimensionless ratio $K = D/H = 5.31$. The same linear variation behavior $A_{lp}{}^{1/2} = KH$ is observed for the average square root area fragments of the directional primary 2D crack domains defined above and denoted by $A_{lp}{}^{1/2}$, with the layer height (see filled triangles in Figure 8). From this, similar dimensionless K values are obtained for 1D and 2D primary cracks.

The K values obtained for the directional and isotropic cracking systems are equal within the experimental errors (5.31 ± 0.25 and 5.42 ± 0.32). Hence, the magnetic field only induces the alignment of the cracks without any effect on the K factor. To our knowledge, this is the first time that the same scaling law is found experimentally for directional and isotropic crack patterns.

Perspectives

The data presented in this Account and those reported in ref 12 clearly show that self-organization of inorganic nanocrystals induces new intrinsic properties (mechanical, optical, magnetic, stability, crystal growth). The nanocrystals self-ordered in 2D and 3D superlattices are highly stable compared with a nanocrystal isolated on a substrate. This opens a new research area, and we need to discover what other physical properties of nanomaterials forming supracrystals can be compared with atoms in the bulk phase. We will ascertain whether the scaling law normally applied for atoms could be also valid for nanomaterials in supracrystals. This will allow us to go further in the analogies between ordered atoms in the bulk phase and nanocrystals and disordered ones and to determine whether the analogies can be made with supracrystals and disordered aggregates, even if the forces involved are not the same. A new question arises: Is this behavior general?

Special thanks are due to my colleagues Drs. A. Courty, N. Goubet, A. I. Henry, I. Lisiecki, A. T. Ngo, D. Parker, and C. Petit. Thanks are also due to Professor E. Duval and Dr. J. Y. Bigot who gave us the opportunity to test our hypotheses and who play a major role in detecting these collective breathing properties of nanocrystals in supracrystals.

BIOGRAPHICAL INFORMATION

Marie-Paule Pileni received a Ph.D. in Physical Chemistry from the University of P&M Curie (UPMC) in 1976. Nominated assistant Professor, she was promoted to associate (1983), full (1990), and distinguished (1997) Professor at UPMC. In 1999, she was nominated member of Institut Universitaire de France (IUF). She received the Langmuir award of the American Chemical Society (1999), the lecture award of the Japanese Chemical Society (2000), the Research Award of the Alexander von Humboldt Foundation in Germany (2003), the Descartes-Huygens Prize of the Royal Netherlands Academy of Arts and Science (2004), and Emilia Valori award from the French Academy of Sciences (2006). She is a member (2004) of the European Academy of Science and the Royal Swedish Academy of Engineering Sciences and has (2002) a doctorate honoris causa from Chalmers University, Göteborg, Sweden. She chairs the Institut Universitaire de France.

REFERENCES

1 Bazylinski, D. A.; Frankel, R. B. Magnetosome formation in prokaryotes. *Nature reviews/microbiology* **2004**, *2*, 217–230.

2 Pileni, M. P. Control of the size and shape of mainly noble inorganic nanocrystals at various scales from nano to macrodomain. *J. Phys. Chem. C* **2007**, *111*, 9019–9038.

3 Whetten, R. L. Crystal structures of molecular gold nanocrystal arrays. *Acc. Chem. Res.* **1999**, *32*, 397–406.

4 Robbins, M. O.; Kremer, K.; Grest, G. S. Phase diagram and dynamics of Yukawa systems. *J. Chem. Phys.* **1988**, *88*, 3286–3312.

5 Bolhuis, P. G.; Frenkel, D.; Mau, S.-C.; Huse, D. A. Entropy difference between crystal phases. *Nature* **1997**, *388*, 235–236.

6 Taylor, A.; Kagle, B. J. *Crystallographic data on metal and alloy structures* Dover Publications: New York, 1963.

7 Hearn, J. E.; Johnston, R. L.; Leoni, S.; Murrell, J. N. Global potentials for calcium and strontium solids. *J. Chem. Soc., Faraday Trans.* **1996**, *92*, 425–432.

8 Kitakami, O; Sato, H.; Shimada, Y.; Sato, F.; Tanaka, M. Size effect on the crystal phase of cobalt fine particles. *Phys. Rev. B* **1997**, *56*, 13849–13854.

9 Tolbert, S. H.; Alivisatos, P. Size dependence of the solid-solid phase diagram in CdSe nanocrystals. *Z. Phys. D* **1993**, *26*, 56–58.

10 Tolbert, S. H.; Alivisatos, P. The wurtzite to rock salt structural transformation in CdSe nanocrystals under high pressure. *J. Chem. Phys.* **1995**, *102*, 4642–4656.

11 Sanders, J. V. Color of precious opal. *Nature* **1964**, *204*, 1151–1153.

12 Pileni, M. P. Self-assembly of inorganic nanocrystals: Fabrication and collective intrinsic properties. *Acc. Chem. Res.* **2007**, *40*, 685–693.

13 Pileni, M. P. Nanocrystal self-assemblies: Fabrication and collective properties. *J. Phys. Chem. B* **2001**, *105*, 3358–3371.

14 Ziherl, P.; Kamien, R. D. Maximizing entropy by minimizing area: towards a new principle of self-organization. *J. Phys. Chem. B* **2001**, *105*, 10147–10158.

15 Henry, A. I.; Courty, A.; Albouy, P. A.; Israelashivili, J.; Pileni, M. P. Tuning of Solid Phase in Supra-crystals made of silver nanocrystals. *Nano Lett.* **2008**, *8*, 2000–2005.

16 Chudnovsky, E. M. Magnetic properties of amorphous ferromagnets. *J. Appl. Phys.* **1988**, *10*, 5770–5775.

17 Chudnovsky, E. M. Dependence of the magnetization law on structural disorder in amorphous ferromagnets. *J. Magn. Magn. Mater.* **1989**, *79*, 127–130.

18 Filippi, J.; Amaral, V.S.; Barbara, B. High field magnetization curve of random anisotropy amorphous magnets: Observation of a crossoverc and link to structural short range order. *Phys. Rev. B* **1991**, *44*, 2842–2845.

19 Thomas, L.; Tuaillon, J.; Perez, J. P.; Dupuis, V.; Perez, A.; Barbara, B. Approach to saturation in nanocrystallized films of iron and nickel. *J. Magn. Magn. Mater.* **1995**, *140–144*, 437–438.

20 Lisiecki, I.; Parker, D.; Salzemann, C.; Pileni, M.-P. Face-centered cubic supra-crystals and disordered three-dimensional assemblies of 7.5 nm cobalt nanocrystals: Influence of the mesoscopic ordering on the magnetic properties. *Chem. Mater.* **2007**, *19*, 4030–4036.

21 Duval, E.; Boukenter, A.; Champagnon, B. Vibration eigenmodes and size of microcrystallites in glass: Observation by very low frequency Raman scattering. *Phys. Rev. Lett.* **1986**, *56*, 2052–2055.

22 Courty, A.; Mermet, A.; Albouy, P.-A.; Duval, E.; Pileni, M.-P. Vibrational coherence of self-organized silver nanocrystals in f.c.c. supra-crystals. *Nat. Mater.* **2005**, *4*, 395–397.

23 Portales, H.; Saviot, L.; Duval, E.; Fujii, M.; Hayashi, S.; Del Fatti, N.; Vallée, F. Resonant Raman scattering by breathing modes of metal nanoparticles. *J. Chem. Phys.* **2001**, *115*, 3444–3447.

24 Duval, E,; Mermet, A.; Courty, A.; Albouy, P. A.; Pileni, M. P. Coherence effect on Raman scattering from self organized Ag-nanocrystals: Theory. *Phys. Rev. B* **2005**, *72*, 85439.

25 Lisiecki, I.; Halte, V.; Petit, C.; Pileni, M. P.; Bigot, J. Y. Vibration dynamics of supra-crystals of cobalt nanocrystals studied with femtosecond laser pulses. *Adv. Mater.* **2008**, *20*, 1–4.

26 Halté, V.; Guille, J.; Merle, J.-C.; Perakis, I.; Bigot, J.-Y. Electron dynamics in silver nanoparticles: Comparison between thin films and glass embedded nanoparticles. *Phys. Rev. B* **1999**, *60*, 11738.

27 Halté, V.; Guille, J.; Merle, J.-C.; Perakis, I.; Bigot, J.-Y. Electron dynamics in silver nanoparticles: Comparison between thin films and glass embedded nanoparticles. *Phys. Rev. B* **1999**, *60*, 11738.

28 Kittel, C. *Introduction to Solid State Physics*, 8th ed.; Wiley and Sons: Hoboken, NJ, 2005.

29 *Nanocrystals Forming Mesoscopic Structures*; Pileni, M. P., Ed.,Wiley: Weinheim, Germany, 2005; Chapter 14.

30 Ngo, A. T.; Richardi, J.; Pileni, M. P. Cracks in magnetic nanocrystal films: do directional and isotropic crack patterns follow the same scaling law? *Nano Lett.* **2008**, *8*, 2485–2489. Ngo, A. T.; Richardi, J.; Pileni, M. P. Do directional primary and secondary crack patterns in thin films of maghemite nanocrystals follow a universal scaling law? *J. Phys. Chem. B.* published online July 30, **2008**, DOI: 10.1021/jp802736g.